SHALE PORE STRUCTURE EVOLUTION AND ITS EFFECT ON PERMEABILITY

T.J. Katsube*, M. Williamson**, and M.E. Best+

*: Geological Survey of Canada, 601 Booth St.
Ottawa, Ontario, K1A 0E8
**: Geological Survey of Canada, Atlantic Geoscience Centre,
PO Box 1006, Dartmouth, Nova Scotia, B2Y 4A2
+: Geological Survey of Canada, Pacific Geoscience Centre,
P.O. Box 6000, Sidney, B.C. V8L 4B2.

ABSTRACT

The effect of compaction and burial on petrophysical characteristics of shales is investigated using shale samples from depths of 1000-4100 m in the Beaufort-MacKenzie Basin and 4500-5600 m in the Scotian shelf. The purpose is to obtain information on permeability and porosity evolution of shales with compaction and burial, to aid studies of hydrocarbon migration and accumulation in Canadian Frontier basins.

Results show that porosity decreases with compaction and burial depth until it reaches a value of 30 % at 1000 m, and continues to decrease to 5 - 10 % at greater depths of 2500 to 4000 m. The pore-structure generally shows a unimodal pore-size distribution, with modes at about 200 nm at 1000 m, which then decreases to 10 - 20 nm at greater depth. The permeabilities, which are in the range of 10^{-14} - 10^{-11} m^2 near the ocean floor surface, decreases to about 10^{-22} - 10^{-20} m^2 at greater depths. At those depths, diagenetic effects on pore structure become significant.

Around 4500-5600 m depth, shale effective porosities and pore-sizes are in the range of 1.5 to 12% and 0.3 nm to 60 µm, respectively. Seventy (70) to 80 % of their porosity is concentrated in the 0.5 to 100 nm range, forming a unimodal distribution of "nano-pores" with modes between 2.7 and 12 nm. While larger pores constitute part of the pathways for fluid flow, the nano-pores constitute the throats, therefore controlling permeability. About 60 % of the nano-pores are fluid-flow paths, except when the final diagenetic phase of the shale is cementation. For such shales, 70-80 % of the nano-porosity is due to dead-ended or larger storage pores.

(245)

INTRODUCTION

Petrophysical information on basin fill is required for quantitative modelling of hydrocarbon charge in Canadian frontier basins (Williamson, 1992). It is the petrophysical properties of shales that determine fluid migration pathways within these basins. Although such information is abundant for sandstones and carbonates, little exists for shales (Mudford and Best, 1989). Indeed, information on permeability and porosity evolution of shales with compaction and burial is essential for these models, since they are designed to reconstruct fluid migration pathways throughout geological time.

Questions regarding shale properties that are important to answer are:

(1)   Why are shale permeabilities extremely low ?, often less than 10^{-20} m^2 (Luffel and Guidry, 1989; Brace, 1980; Morrow et al., 1984; Mudford and Best, 1989).

(2)   How does diagenesis influence shale permeabilities ?

(3)   What are the shale overpressure mechanisms ?

(4)   How does compaction and burial affect shale permeabilities ?

Answers to these questions will provide information on the evolution of pore structure and its effect on permeability as muds are transformed into shale through compression and heating during their subsidence history.

Katsube et al. (1991a) obtained permeabilities of 10^{-22} - 7×10^{-22} m^2 for a suite of tight shale samples from depth of 4500 - 5600 m in the Venture Gas Field, offshore Nova Scotia, and indicated that these low permeabilities are due to the shale interconnected pore network consisting of extremely tortuous (true tortuosity = 3.3) and small pores. These pores, nano-pores, appear as a unimodal distribution of pore-sizes in the 2.5-60 nm range with a mean of about 8-16 nm (Katsube et al., 1991a). Since the nano-pores play a dominant role in determining the petrophysical properties of shales, a comprehensive description of their characteristics (Katsube, 1992) is given in this paper.

This paper describes how the nano-pores are thought to have developed into their present form under increasing pressure due to compaction and burial, how diagenesis affects these pores, and how the nano-pores influence tight shale permeability and porosity. The results are based on recent studies being carried out on the petrophysical characteristics of shale samples from Canadian Frontier Basins (Katsube et al., 1991a; Coyner, et al., 1992; Katsube and Best, 1992; Katsube et al., 1992a, 1992b; 1992c). The measurement and analytical techniques used in these studies include shale texture analysis (mineralogical and texture analysis), effective porosity (ϕ_E) and formation factor (F) measurements, electrical resistivity (bulk and surface resistivity: ρ_o, ρ_R), mercury porosimetry (Pore-size distribution), permeability (k) measurements, crack-porosity (ϵ), measurements, and petrographic image analysis (PIA). The mineralogical and texture analysis include X-ray diffraction (XRD), scanning electron microscopy (SEM) and petrographic thin section analysis (PTA).

NANO-PORE STRUCTURE

Typical examples of the pore-size distribution for tight shales from the Venture Gas Field are shown in Figure 1, with the concentration of porosity in the 2.5 - 60 nm range, forming the unimodal distribution of nano-pores. Compare these results to those of crystalline rocks illustrated in Figure 2, which is not a unimodal distribution. It was suggested that the nano-pores are important (Katsube et al., 1991a) not only because of the porosity concentrated in them, but also because indications are they form the major fluid-flow paths. Average pore-sizes, d_{Fk}, of the fluid flow paths determined from the permeabilities (k) and formation factor (F) values (6.5 - 9.3 nm) using the Walsh and Brace(1984) equation:

$$d_{Fk} = \sqrt{12Fk}, \qquad\qquad (1)$$

were comparable with the geometric means, d_{hg}, (10.0 - 13.1 nm) of the pore-size distribution derived from the mercury porosimetry measurements (Katsube, et al., 1991a), and with the nano-pore modes, d_{np}, (2.5 - 10 nm). The pore-sizes above 25 nm do not significantly contribute to the flow paths, although they may be part of the inter-connected pore-structure network. They are either few in number or are blind (or pocket) pores.

The minimum pore-size measured by mercury porosimetry used in these studies (Katsube et al., 1991a) was 2.5 nm. However, there were strong indications that pores exist below that limit (Figure 1). Therefore, a normal distribution curve was fitted (Katsube, 1992) to the pore-size distribution data of 10 shale samples from the Venture Gas Field offshore Nova Scotia (Katsube, et al., 1991a) to estimate the missing porosity, $\Delta\phi$, contained in these pores. It was assumed that they constitute part of a unimodal distribution of nano-pores.

Some of the results are listed in Table 1. The parameter ϕ_{Eg} is used instead of ϕ_E in this table because it is obtained from actual measurements of ϕ_{gm} and estimations of $\Delta\phi$, which is not necessarily equivalent to the ideal or conceptual effective porosity (ϕ_E):

$$\phi_{Eg} = \phi_{gm} + \Delta\phi. \tag{2}$$

These results show that missing porosity ($\Delta\phi$) values are in the range of 0.2-4.0 %. This is about 12-36 % of the nano-pore porosity (ϕ_{np}), which occupies 83±4 % of the effective porosity (ϕ_{Eg}), the porosity of all interconnected pores in the shales. Therefore, missing porosity determination significantly improved the measurement accuracy. The nano-pore porosities (ϕ_{np}) were in the range of 1.5 - 10.2 % for these samples. The results also show that nano-pore sizes (d) are in the range of 0.2 - 100 nm, and their modes (d_{np}) in the range of 2.7-11.5 nm, the smallest known values for rocks. The porosity data of ϕ_{np}, ϕ_{gm}, $\Delta\phi$ and ϕ_{Eg} for all Venture Gas Field samples are listed in Table 1. The nano-pore characteristics of the same samples represented by d_{np}, σ, ϕ_{max} and d_{hg} are listed in Table

2. The parameters σ and ϕ_{max} are the standard deviation (based on log of d) and maximum nano-pore partial porosity, respectively.

EFFECT OF COMPACTION AND BURIAL

Permeability (k), Porosity (ϕ_E), Formation-Factor (F), Mercury porosimetry (ϕ_a) measurements and Shale Texture Analysis (XRD, SEM, PTA) are being carried out on shale samples taken at depths of 1000 - 4100 m in the Beaufort-MacKenzie Basin offshore North West Territories, in order to study the effect of compaction on porosity, pore structure and pore-size distribution of shales.

The results (Katsube and Best, 1992; Katsube et al., 1992c) show a unimodal distribution of pore-sizes, similar to those from the Venture Gas Field, but with larger porosities and mean pore-sizes at shallower depth (Figure 3). The porosity (ϕ_{gm}) decrease with compaction and burial depth reaches a value of 30 % at 1000 m, and continues to decrease to 5 - 10 % at the greater depths of 2500 to 4000 m, thus supporting the reported linear porosity versus depth relationship (Issler, 1992). The modes of the unimodal pore-size distribution are about 200 nm at 1000 m, which decreases to 10 - 20 nm at greater depths (Figure 3). The permeabilities, which are in the range of 10^{-14} - 10^{-11} m^2 near the ocean floor surface (Katsube et al., 1991b), decrease to about 10^{-22} - 10^{-20} m^2 (Katsube et al., 1991a; Coyner et al., 1992) at greater depth, a 6 to 10 orders of magnitude decrease due to burial.

EFFECT OF DIAGENESIS

Shale Texture Analysis (XRD, SEM, PTA) were made on 10 shale samples taken at depths between 4500 m and 5600 m in 3 wells on the Scotian shelf, in order to study the effect of diagenesis on pore-structure of tight shales (Katsube et al., 1992a,b). These samples have been subjected to a series of diagenetic cementation and dissolution cycles.

The results show that samples characterized by late-stage cementation have small effective porosities of 1.5 to 2.5 %, while shales with the final diagenetic phase being dissolution have porosities of 8-12%. These tight shale and shaly samples were obtained from formations that have been subjected to a number of diagenetic processes consisting of alternating phases of cementation and dissolution. The larger pores (d>25 nm) represent primary intergranular pores, secondary grain-moldic and intra-granular pores, or throats leading to these pores. The larger nano-pores represent intercrystalline micro-pores (also d>25 nm) and throats that lead to larger pores. The nano-pores represent the interconnected network of fluid-flow pathways which are thought to be associated with the clay matrix minerals and microcrystalline pore filling cement. These relationships between pore-structure and diagenesis can be seen in Figure 4. The presence of calcite and dolomite generally imply that the final diagenetic phase of the sample is cementation.

The results (Katsube et al., 1992b) also show that while early cements consisting of pyrite, calcite and quartz, most likely form the framework of the nano-pores, there is no evidence that a difference in these cement types cause variations in the nano-pore structure. However, the existence of the late dolomitic pore filling cement has a striking effect by blocking the nano-pores (Figure 4), thus reducing the nano-pore porosity considerably. Dolomite cement also has a significant effect on the effective porosity (ϕ_E) as small quantities reduce the porosity values considerably. The late calcite and siderite pore filling cements have similar effects, but not as striking as the dolomite.

Samples with a final diagenetic phase consisting of cementation show small effective and nano-pore porosities, 1.5-2.8 % and 1.5-2.4 %, respectively (Katsube et al.,

1992b). These results also show that the majority of the larger pores are filled with cement, and about 70-80 % of the nano-pores are blocked. Samples with a final diagenetic phase consisting of dissolution show effective porosities of 8-12% with contributions from various types of open storage pores. The maximum porosity potential of these shales, attained at advanced stages of a dissolution phase, appears to be 10-12%, with the larger porosities occurring at earlier dissolution periods. There appears to be a very limited number of occluded or residual pores, that is pores which are entirely cut off from the interconnected pore network.

LOW PERMEABILITY MECHANISM

Recent petrophysical studies on shales has provided an insight into their low permeability mechanism in three areas, namely (1) water penetrates the smallest pores that are detected in these shales (Katsube, 1992), (2) the nano-pores form the main interconnected pore network and the major pore throats (Katsube et al., 1991a; Katsube et al., 1992a,b), and (3) a critical nano-pore porosity exists below which the availability of flow paths rapidly decrease with decreasing nano-pore porosity (Katsube et al., 1992a,b).

In Katsube (1992), the estimated effective porosity (ϕ_{Eg}) values (Table 1) are shown to have a relatively good correlation with the reported values of effective porosity, ϕ_{EI}, measured by the immersion technique (Katsube et al., 1992d), as shown in Figure 5. The fact that this correlation is a considerable improvement over that of ϕ_{gm} and ϕ_{EI}, indicates that the inclusion of the missing porosity ($\Delta\phi$) in the estimated effective porosity (ϕ_{Eg}) calculations considerably improves the accuracy of the porosity measurements by mercury porosimetry. The effective porosity (ϕ_{EI}) obtained by the immersion technique was determined by taking the difference in mass between an oven-dried rock specimens

and the same specimen saturated with water (Katsube and Scromeda, 1991; Katsube et al., 1992d). The fact that the two porosities, ϕ_{Eg} and ϕ_{EI}, are strongly correlated suggests that water penetrates the pores smaller than the minimum pore-size measurable by mercury porosimetry, i.e., those not included in the mercury porosimetry data. That is, water penetrates and can be evacuated from all of the nano-pores. The minimum pore-size value obtained from fitting the normal distribution curve (Katsube, 1992) is 0.2 nm. This value is smaller than many ions in the pore water, so a problem exists in explaining how water can penetrate the nano-pores under these conditions.

Histograms for the mean pore-sizes d_{FI}, d_{np} and d_{hg}, are displayed in Figure 6. The mean pore-size, d_{FI}, represents the mean pore-size of the flow paths for fluids and electrical current. The fact that its distribution resembles that of d_{np} rather than d_{hg}, is interpreted to indicate that the nano-pores form the main interconnected pore path network for fluid flow, and that the larger pores do not control the permeability, although they may be part of the interconnected pore path network. This supports the results by Katsube et al. (1991a).

The electrical porosity, ϕ_F, represents the porosity of the pores that contribute to the flow of electrical current, and most likely fluids as well (Katsube et al., 1992a,b). It is derived from

$$\phi_F = \tau^2/F, \qquad\qquad (3)$$

where F is the formation factor and τ is the true   tortuosity (Katsube et al., 1992b). A value of $\tau = 3.3$ has been used in accordance with the results obtained by Katsube et al. (1991a). The relationship between ϕ_F and the nano-pore porosity (ϕ_{np}) is displayed in Figure 7 (Katsube et al., 1992a,b). This relationship is generally interpreted to be linear (broken line) with an intercept at ϕ_{np}=1.0-1.5 %. Sample number 4 has been excluded from the diagram, because it shows a considerable deviation from the rest of the data. This intercept is the first critical nano-pore porosity, ϕ_{np1}, whose existence implies there

are few or no flow paths through the rock for nano-pore porosities (ϕ_{np}) below that value. Namely, water or mercury can enter the pores on the specimen surface, but can not flow through the rock from one end to the other for nano-pore porosities below that value.

There is a deviation from the linear relationship (broken line) between the two porosities (ϕ_F and ϕ_{np}) for nano-pore porosities (ϕ_{np}) between 2.5 and 6.0 %. The linear relationship for $\phi_{np} > 6.0$ % indicates that 50-60 % of the nano-pore porosity (ϕ_{np}) is contained in interconnected paths available for flow of fluids and electrical current. The linear relationship breaks down for $\phi_{np} < 6.0$ %, that is below the second critical nano-pore porosity, ϕ_{np2} (=6.0 %), with ϕ_F falling below 50-60 % of ϕ_{np}. This implies that the relatively good interconnectivity of the flow path network that existed at larger nano-pore porosities, breaks down for $\phi_{np} < 6.0$ % and that more of the nano-pores become disconnected and end up as pocket or blind pores at these porosities. This second critical nano-pore porosity (ϕ_{np2}) is the point of transition, from the state where many of the nano-pores that were fluid-flow paths at the higher porosities become blocked or dead-ended at the lower porosities, and is the point where the final diagenetic phase changes from being dominantly dissolution to that which is dominantly cementation.

DISCUSSION AND CONCLUSIONS

Results of recent studies show that at 4500-5600 m depth, shale effective porosities and pore-sizes are in the range of 1.4 to 12% and 0.3 nm to 60 µm, respectively. Seventy (70) to 80 % of their porosity is generally concentrated in the 0.5 to 100 nm range, forming a unimodal distribution of "nano-pores" with modes between 2.7 and 11.5 nm. While larger pores constitute part of the pathways for fluid flow, the nano-pores constitute the throats, therefore controlling permeability. About 60 % of the nano-pores

are fluid-flow paths, except when cementation is the final diagenetic phase of the shale. For such shales, 70-80 % of the nano-pore porosity is due to dead-ended or larger storage pores. The nano-pores appear to constitute an interconnected pore network within the pore filling cement. Well cemented shales have small porosities of 1.5 to 2.5%, with approximately 70-80 % of the nano-pores being blocked. It appears that water can penetrate and be evacuated (ie. imbibed and drained) from all the nano-pores.

On the other hand, results of a study involving shales taken from a depth of 1000 - 4000 m also show a unimodal pore-size distribution. The characteristics of the distribution change considerably with degree of compaction and burial. The modes of the unimodal pore-size distribution are about 200 nm at 1000 m, and decreases to 10 - 20 nm at a depth of 4000 m. The effective porosity decreases with compaction and burial depth. It reaches a value of 30 % at 1000 m, and continues to 5 - 10 % at greater depths of 2500 to 4000 m. The permeabilities, which are in the range of 10^{-14} - 10^{-11} m^2 near the ocean floor surface, decrease to about 10^{-22} - 10^{-20} m^2 at greater depths, a 6 to 10 orders of magnitude decrease due to burial. At that depth, diagenetic and overpressure effects on pore structure become significant.

ACKNOWLEDGEMENTS

REFERENCES

Agterberg, F.P., Katsube, T.J., and Lew, S.N., 1984, Statistical analysis of granite pore size distribution data, Lac du Bonnet batholith, eastern Manitoba: Current research, Part A, Geological Survey of Canada, Paper 84-1A, 29-38.

Brace, W.F., 1980, Permeability of crystalline and argillaceous rocks: Int. J. Rock Mech. Min. Sci. & Geomech. Abstr. 17, 241-251.

Issler, D.R., 1992, A new approach to shale compaction and stratigraphic restoration, Beaufort-MacKenzie Corridor, Northern Canada: in press (AAPG).

Coyner, K., Katsube, T.J., Williamson, M., and Best, M.E., 1992, Gas and water permeability of tight shales from the Venture Gas field, offshore Nova Scotia: in preparation for publication in Geological Survey of Canada, Paper 92-E.

Katsube, T.J., 1981, Pore structure and pore parameters that control the radionuclide transport in crystalline rocks: Proceedings of the Technical Program, International Powder and Bulk Solids Handling and Processing, Rosemont, Illinois, 394-409.

Katsube, T.J., 1992, Statistical analysis of pore-size distribution data for tight shales from the Scotian Shelf: in preparation for publication in Geological Survey of Canada, Paper 92-E.

Katsube, T.J., and Scromeda, N., 1991, Effective porosity measuring procedure for low porosity rocks: Geological Survey of Canada, Paper 91-E, 291 -297.

Katsube, T.J., Best, M.E., and Mudford, B.S., 1991a, Petrophysical characteristics of shales from the Scotian shelf: Geophysics, 56, 1681-1689.

Katsube, T.J., Wires, K., Cameron, B.I., and Franklin, J.M., 1991b, Porosity and permeability of ocean floor sediments from the Middle Valley Zone in the northeast Pacific; Borehole PAR90-1: Geological Survey of Canada, Paper 91-E, 91-97.

Katsube, T.J., Williamson, M., Murphy, T.B., and Best, M.E., 1992a, Relationship between pore structure and diagenetic processes of tight shales from the Scotian Shelf: Presented at the GAC-MAC Joint Annual Meeting, May 25-27, 1992, Wolfville, Nova Scotia.

Katsube, T.J., Murphy, T.B., Williamson, M., and Best, M.E., 1992b, Relationship between pore structure and diagenetic processes of tight shales from the Scotian Shelf: in preparation for publication.

Katsube, T.J., Williamson, M., Issler, D.R., and Best, M.E., 1992c, Petrophysical properties of shales; Significance for modelling sedimentary basins: Poster paper presented at the "GSC Oil and Gas Forum '92", Calgary, Alberta, March 2-3, 1992.

Katsube, T.J., Scromeda, N., and Williamson, M., 1992d, Effective porosity of tight shales from the Venture Gas Field, offshore Nova Scotia: Geological Survey of Canada, Paper 92-1D, 111-119.

Katsube, T.J., and Best, M.E., 1992, Pore structure of shales from the Beaufort-MacKenzie Basin, Geological Survey of Canada, Paper 92-E.

Luffel, D.L., and Guidry, F.K., 1989, Reservoir rock properties of Devonian shale from core and log analysis: The Society of Core Analysts, Annual Technical Conference Preprints, Vol. I, Aug. 2-3, Paper 8910.

Morrow, C., Shi, L., and Byerlee, J., 1984, Permeability of fault gauge under confining pressure and shear stress: J. of Geophys. Res., 89, 3193-3200.

Mudford, B.S., and Best, M.E.,1989, Venture Gas Field, offshore Nova Scotia; case study of overpressuring in region of low sedimentation rate: Bull. AAPG, 73, 1383-1396.

Walsh, J.B., and Brace, W.F.,1984, The effect of pressure on porosity and the transport properties of rocks. Journal of Geophysical Research, 89, 9425-9431.

Williamson, M.A., 1992, Hydrocarbon resource study of east coast frontier basins; past present and future (Abstract): In Geological Survey of Canada, Current Activity Forum, Program with Abstracts, 4.

Table 1: List of various porosities (Katsube, 1992; Katsube et al., 1992b).

Sample	ϕ_{np}	ϕ_{gm}	$\Delta\phi$	ϕ_{Eg}	ϕ_{EI}	ϕ_{F}
V-1	5.53	4.9	1.52	6.42	6.0	2.2
V-2	6.61	7.7	0.34	8.04	5.7	3.7
V-3	6.97	6.3	1.86	8.16	8.6	4.2
V-4	10.2	7.6	3.95	11.5	12.1	2.1
V-5	4.52	3.7	2.12	5.82	5.3	1.1
V-6	1.53	1.6	0.18	1.78	1.4	0.07
V-7	5.83	5.9	1.16	7.1	8.6	2.7
V-8	8.37	9.1	1.20	10.3	12.1	4.7
V-9	2.35	2.3	0.50	2.8	1.5	0.7
V-10	5.83	5.8	1.55	7.3	8.2	3.4
Units	%	%	%	%	%	%

ϕ_{np} = Nano-pore porosity.

ϕ_{gm} = Total porosity measured by mercury porosimetry.

$\Delta\phi$ = Estimated missing porosity.

ϕ_{Eg} = Estimated effective porosity by mercury porosimetry: $\phi_{Eg} = \phi_{gm} + \Delta\phi$, (Katsube et al., 1992b).

ϕ_{EI} = Effective porosity measured by immersion technique using long oven drying time (from Katsube et al., 1992d).

ϕ_{F} = Electrical porosity ($\phi_{F} = \tau^2/F$, $\tau = 3.3$, τ = true tortuosity), the porosity derived from formation factor (Katsube et al., 1992b).

Table 2: Nano-pore characteristics of the shale samples from the Venture Gas Field (after Katsube, 1992; Katsube et al., 1992-in prep.).

Sample	d_{np}	σ	ϕ_{max}	d_{hg}	d_{Fk}
V-1	4.41	0.412	1.07	10.0	6.24
V-2	11.5	0.412	1.26	16.2	5.02
V-3	5.61	0.566	0.983	13.3	-
V-4	3.51	0.520	1.56	11.1	13.7
V-5	2.73	0.500	0.721	13.6	5.06
V-6	5.88	0.316	0.386	8.7	23.1
V-7	5.58	0.412	1.13	9.5	-
V-8	6.82	0.412	1.62	11.9	9.06
V-9	5.70	0.447	0.42	10.0	7.02
V-10	4.75	0.447	1.04	13.1	9.01
Units	nm		%	nm	nm

d_{np} = nano-pore mode

σ = standard deviation (based on log of d)

ϕ_{np} = nano-pore porosity

ϕ_{max} = maximum nano-pore partial porosity

d_{hg} = mean pore-size of the pore-size distribution measured by mercury porosimetry

d_{Fk} = mean pore-size of the flow paths derived from permeability (k) and formation factor (F) measurements (after Katsube et al., 1992-in prep.)

CAPTIONS FOR ILLUSTRATIONS

Figure 1: Typical pore-size distributions in terms of partial porosity (ϕ_a) for (a) Sample number 6 (5131.5 m), and (b) Sample number 10 (5557.0 m), (after Katsube et al., 1991). Partial porosity (ϕ_a) is the porosity contributed by each pore-size range (e.g. 2.5-4.0 nm, 4.0-6.3 nm).

Figure 2: Pore size distribution for a suite of crystalline rocks (Katsube, 1981: Agterberg et al., 1984).

Figure 3: Pore-size distribution change with depth, with modes at about 200 nm at 1000 m decreasing to 10 - 20 nm at the greater depth.

Figure 4: Results of pore-size (d) distribution in terms of partial porosity (ϕ_a), formation-factor (F), effective porosities ϕ_{EI} and ϕ_{gm}, and mineralogy for the 10 samples (Katsube et al., 1991; Katsube et al., 1992b). The partial porosity (ϕ_a) range for for all samples is 0.01-1.0%, as shown for sample number 10. Partial porosity (ϕ_a) is the porosity contributed by each pore-size range (e.g. 2.5-4.0 nm, 4.0-6.3 nm).

Figure 5: Estimated effective porosity (ϕ_{Eg}) and total porosity (ϕ_{gm}) as a function of effective porosity (ϕ_{EI}) for the 10 shale samples (after Katsube, 1992). The functional relationships between ϕ_{Eg} versus ϕ_{EI}, and ϕ_{gm} versus ϕ_{EI} are as follows:
$$\phi_{Eg} = (0.80 \pm 0.04)\phi_{EI} + (1.0 \pm 0.3), \quad r=0.96,$$
$$\phi_{gm} = (0.64 \pm 0.08)\phi_{EI} + (1.0 \pm 1.4), \quad r=0.88,$$
where r is the correlation factor. The one-point broken line represents $\phi_{Eg} = \phi_{EI}$.

Figure 6: Histograms for the mean pore-sizes d_{Fk}, d_{np} and d_{hg}.

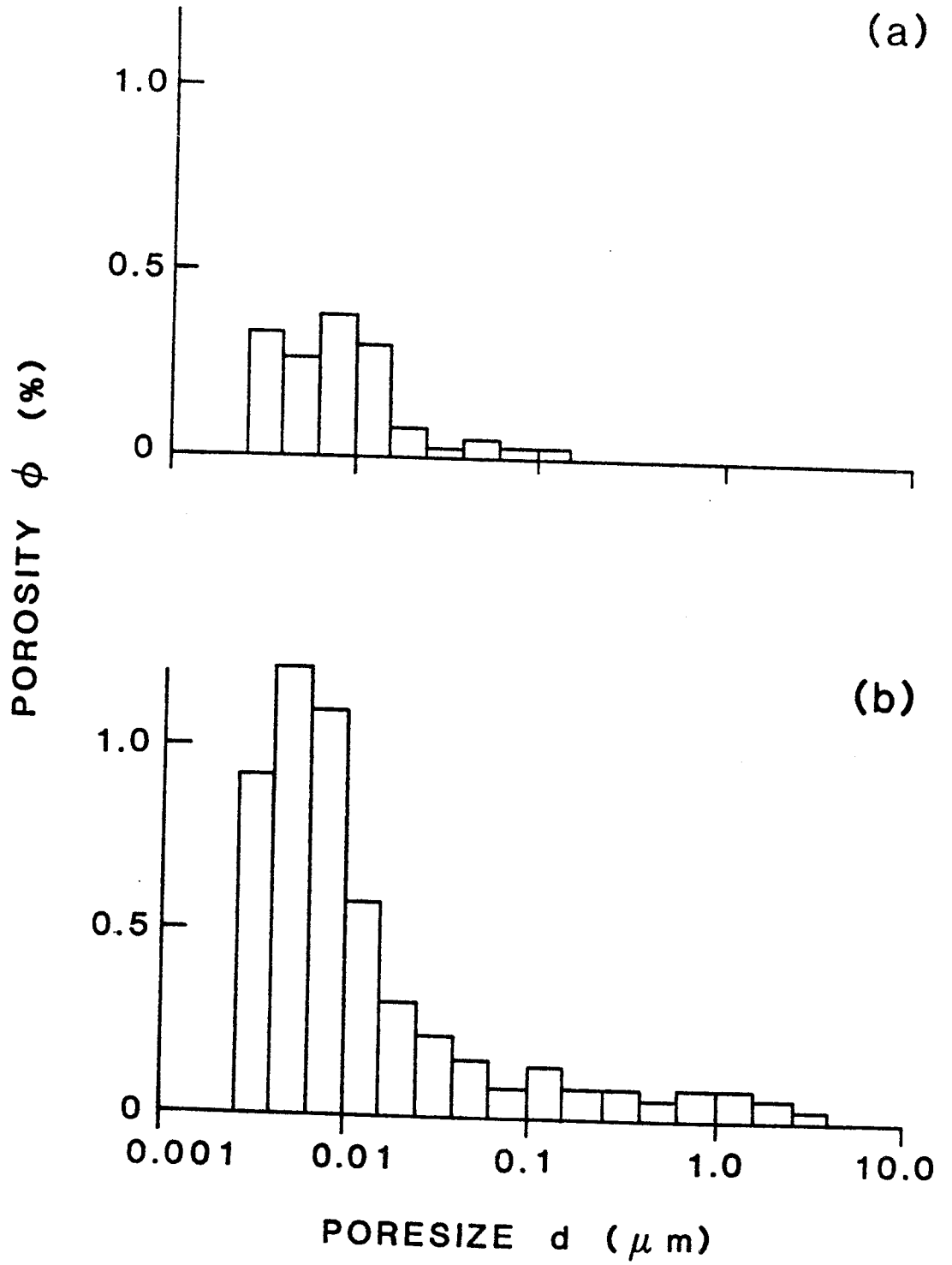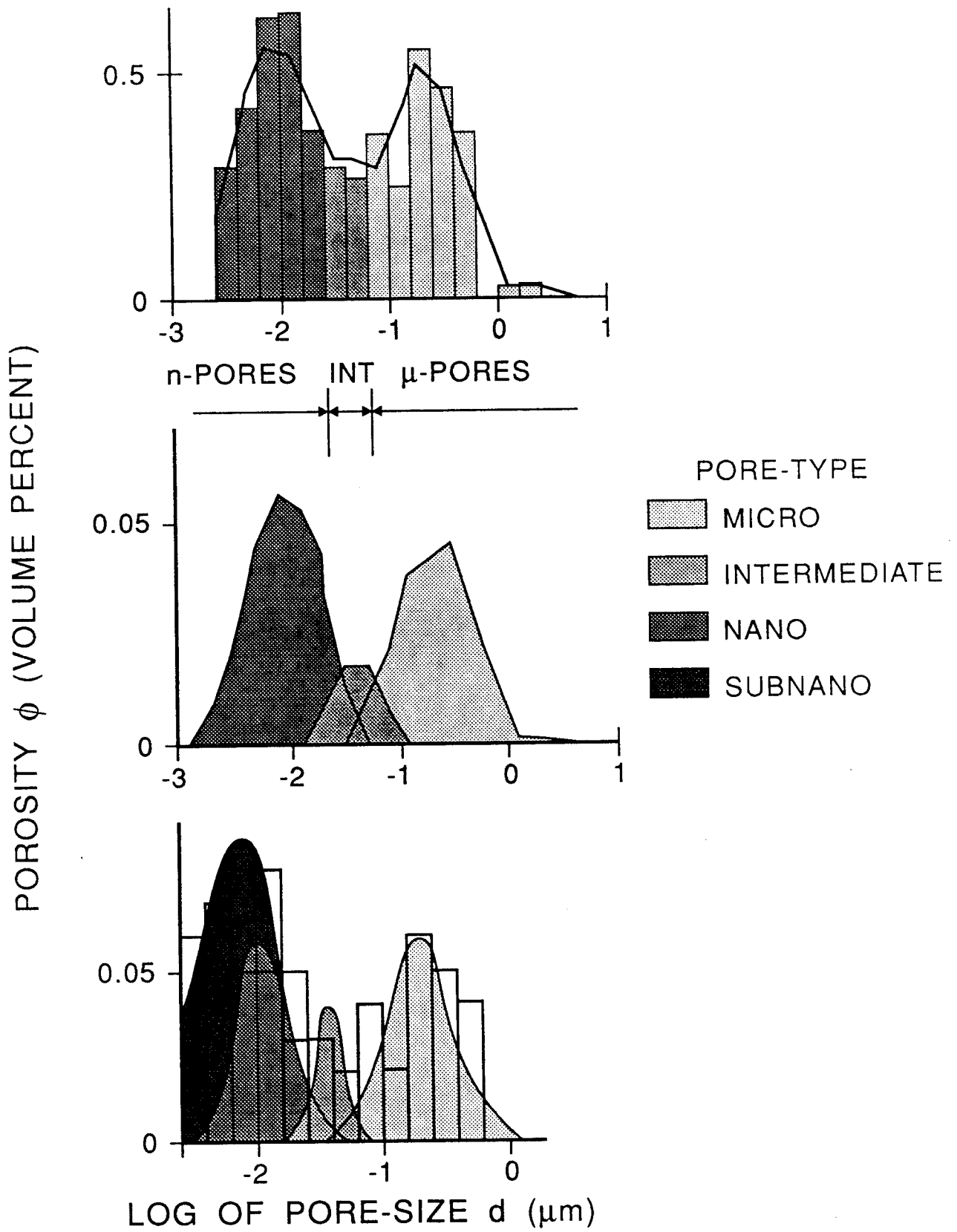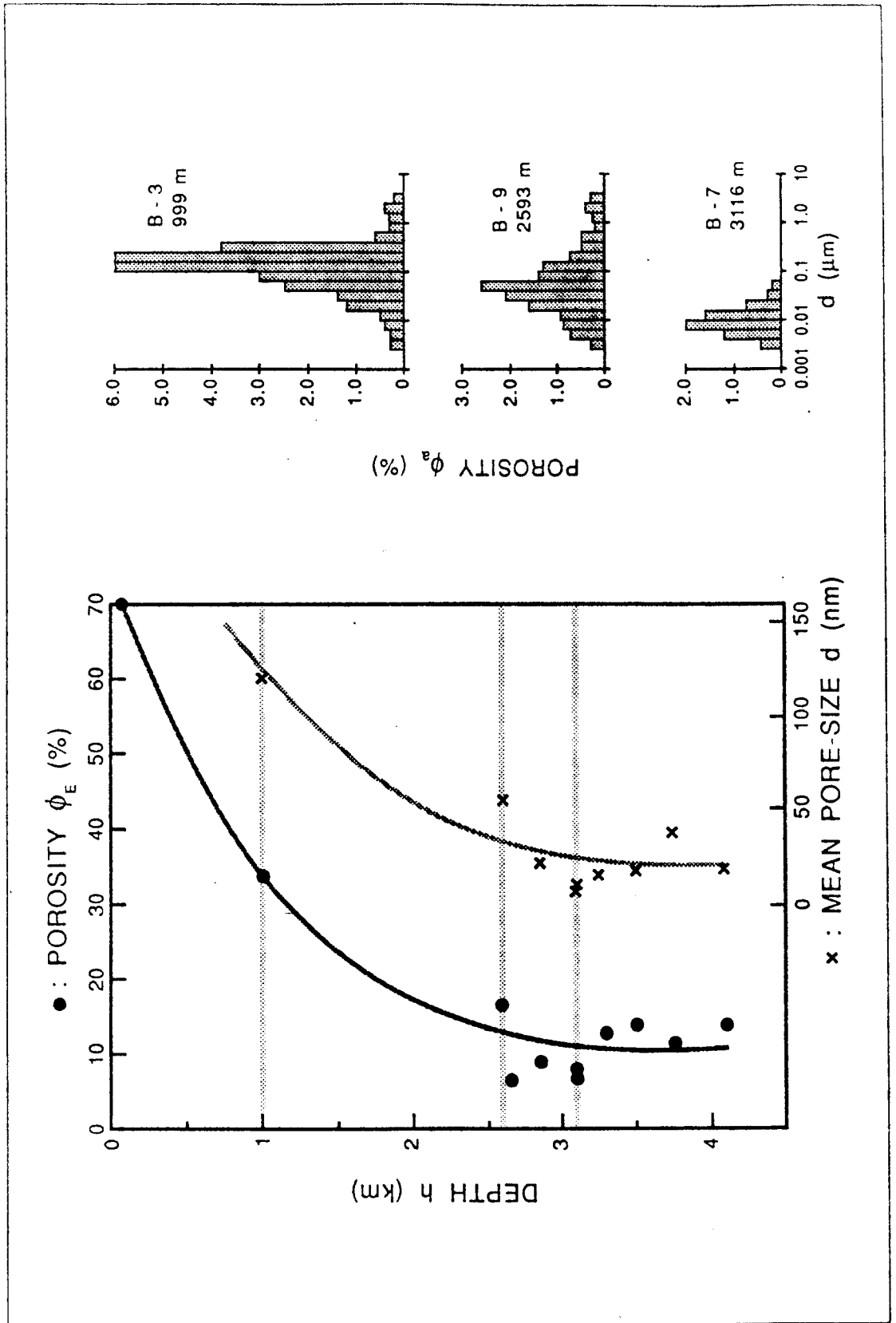**Figure 7:** The relationship between electrical porosity (ϕ_F) and nano-pore porosity (ϕ_{np}).
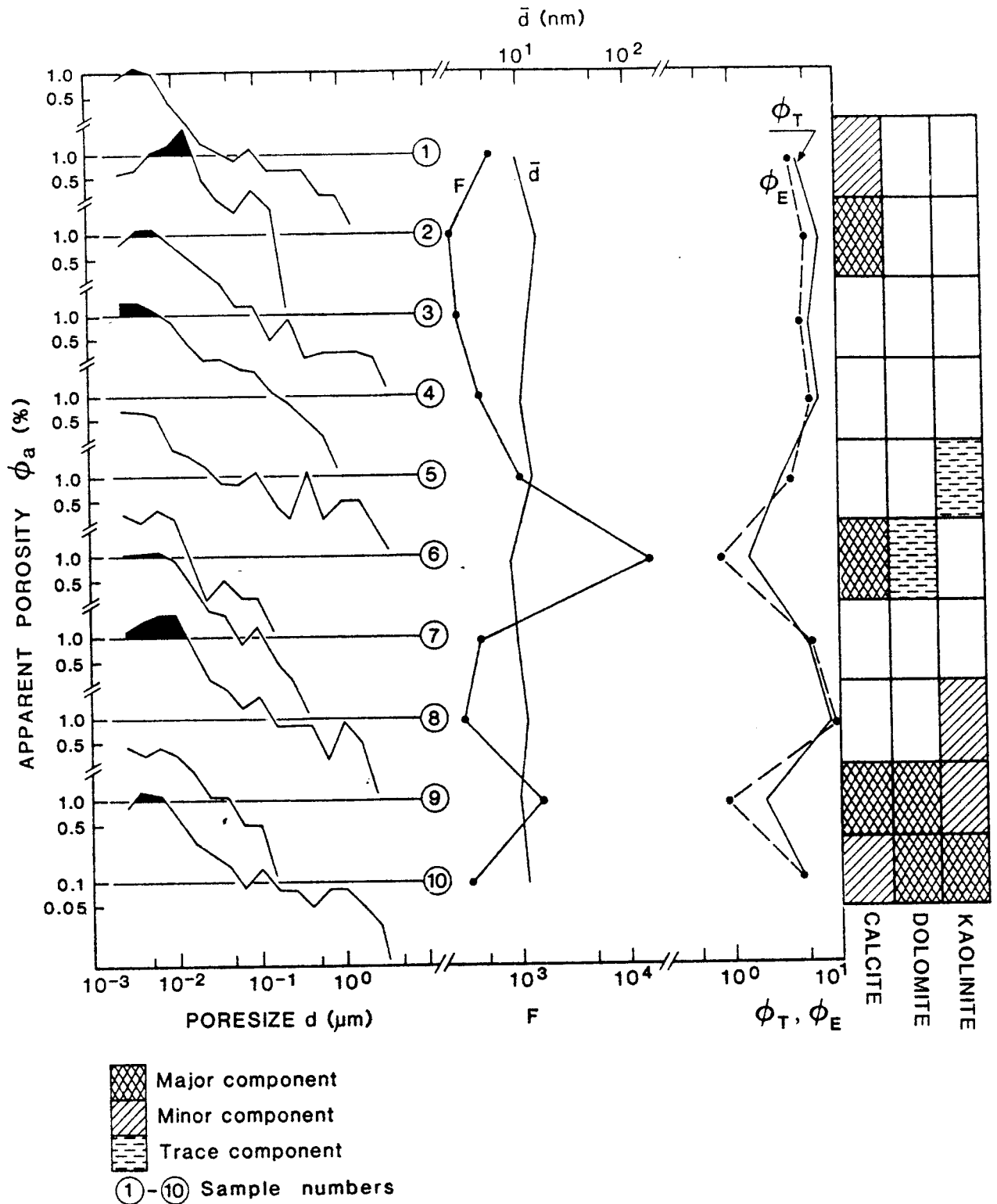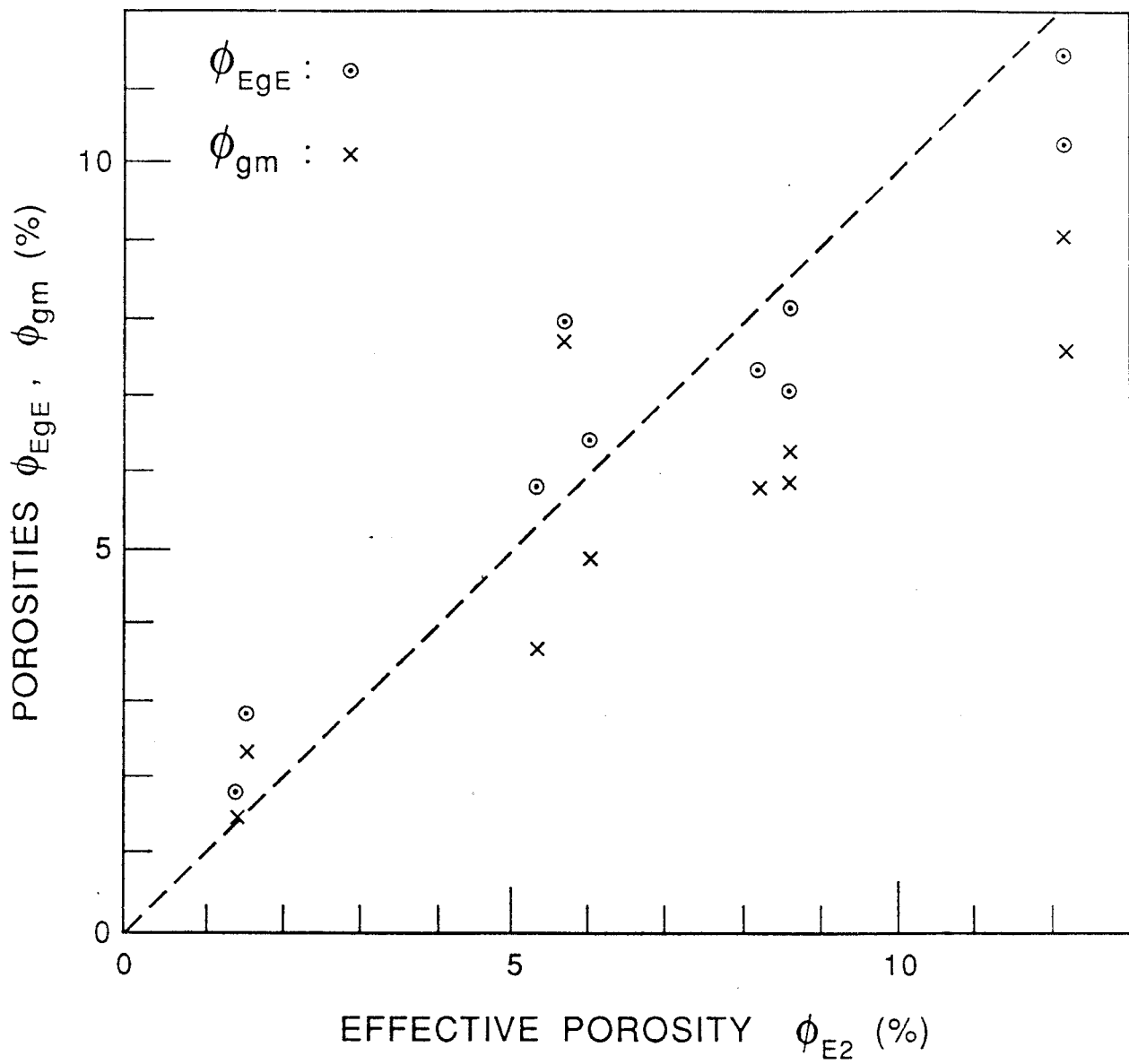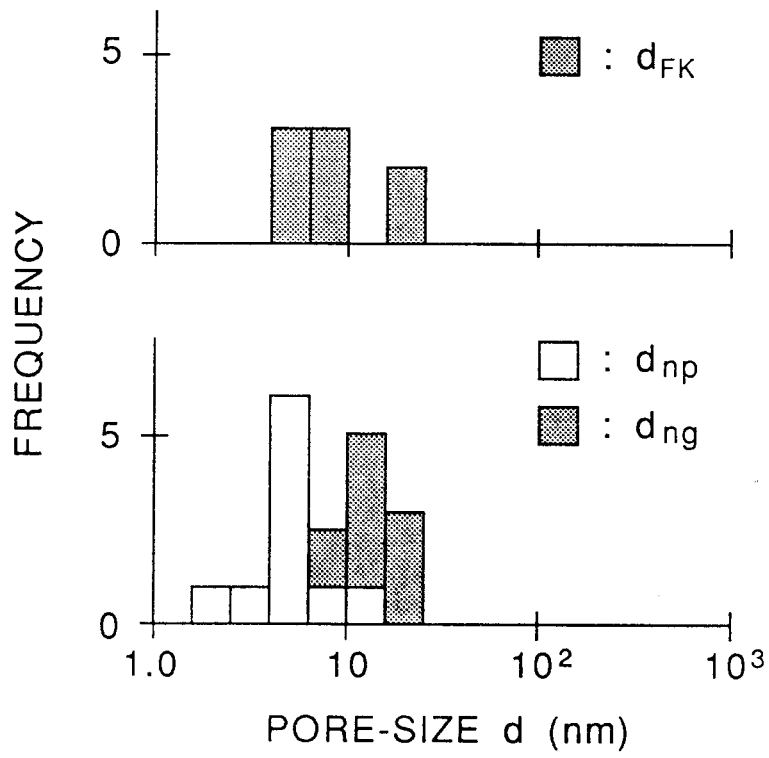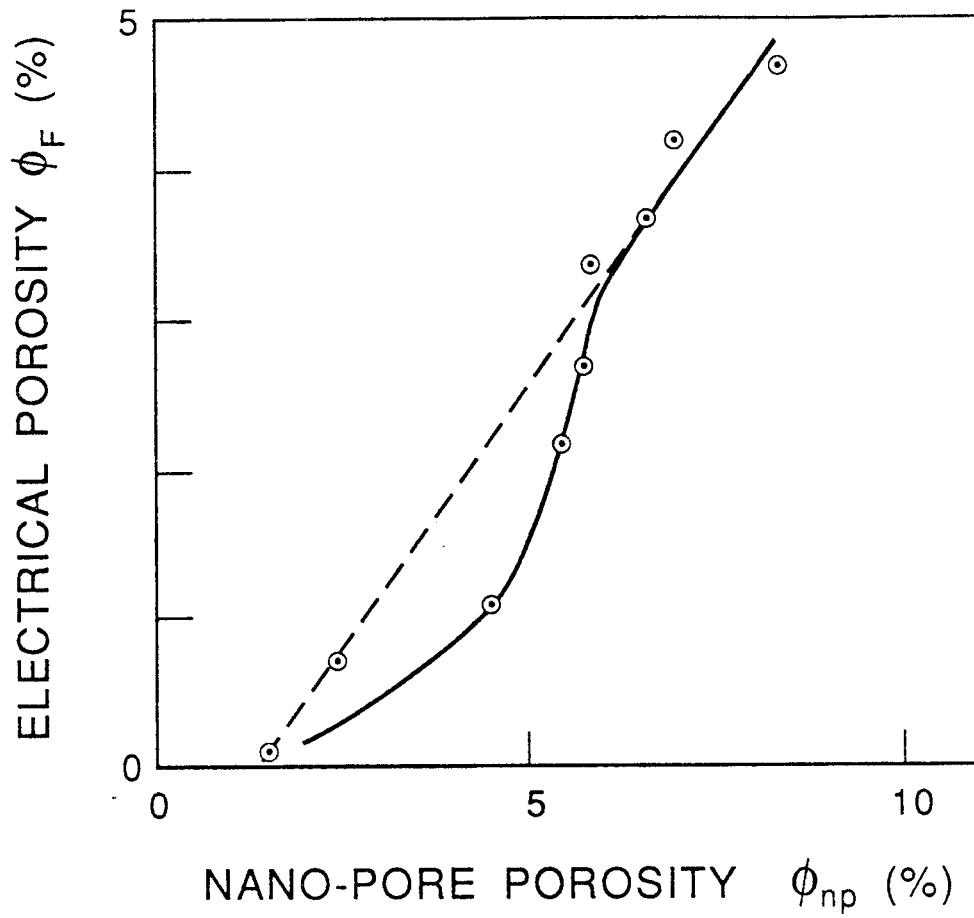
(3908)

15

Figure 1.

Figure 2.

Figure 3.

Figure 4

Figure 5

Figure 6

Figure 7.